2

CONF-860756--6

UCRL-94583
PREPRINT

FREE ELECTRON LASER AMPLIFIER DRIVEN BY AN INDUCTION LINAC

V. K. Neil

UCRL--94583
DE88 002452

This paper was prepared for submittal to

High-Brightness Accelerators
Pitlochry, Scotland

July 13-25, 1986

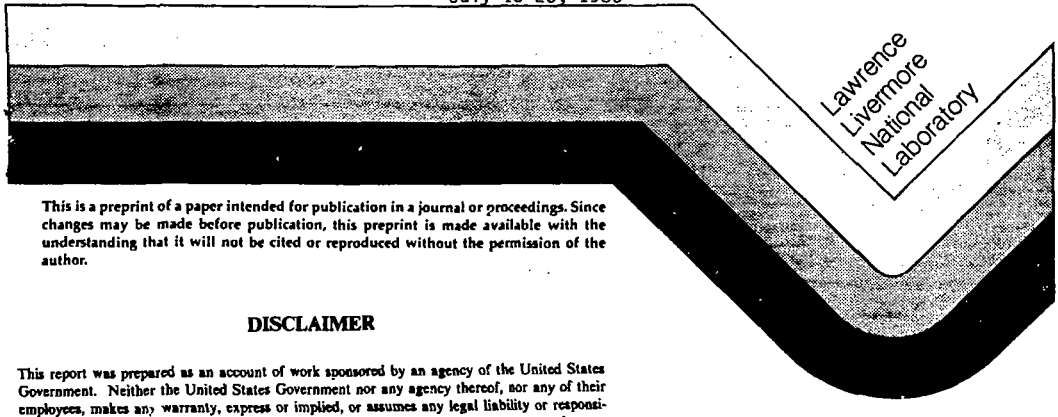

FREE ELECTRON LASER AMPLIFIER DRIVEN BY AN INDUCTION LINAC*

V. Kelvin Neil
Lawrence Livermore National Laboratory
P. O. Box 808, L-626
Livermore, CA 94550

June 3, 1986

I. INTRODUCTION

A free-electron laser (FEL) directly converts the kinetic energy of a high-brightness, relativistic electron beam into coherent radiation. It is a classical device, much like a traveling wave tube. In an FEL amplifier the conversion takes place in a single pass through a wiggler magnet, therefore the fraction of kinetic energy converted must be high if the device is to be efficient. Since the conversion is a rapidly increasing function of the electron beam current, a current of 1 kA or greater is desired. The particle energy required depends on the wavelength of coherent radiation. For a given wiggler wavelength, λ_w, wiggler magnetic field B, and radiation wavelength λ_s, there is a resonance condition that determines the proper electron energy. This condition will be derived in Sec. 3, and is

$$\lambda_s = \frac{\lambda_w}{2\gamma^2}\left[1 + \frac{1}{2}\left(\frac{eB\lambda_w}{2\pi mc^2}\right)^2\right] , \qquad (1.1)$$

in which γ is the electron energy in units of the rest energy, mc^2. If B and λ_w do not vary with position as the particle's energy is converted and γ decreases, the condition is no longer satisfied at some position, and saturation results. However, if B or λ_w or some combination varies with axial position, the resonance condition can be maintained. The conversion efficiency

* Work performed jointly under the auspices of the U. S. Department of Energy by Lawrence Livermore National Laboratory under contract W-7405-ENG-48, for the Strategic Defense Initiative Organization and the U. S. Army Strategic Defense Command in support of SDIO/SDC-ATC MIPR No. W31-RPD-63-A072.

(also called extraction efficiency) is greatly enhanced and the output radiation energy increased. A device in which B/λ_w varies is called a variable parameter wiggler, or a tapered wiggler. An experiment called ELF (electron laser facility) is a device with $\lambda_w = 9.8$ cm, $\lambda_s = 8.6$ mm and $\gamma = 8$. The experiment is described in Sec. 4. Experimental results for both untapered and tapered configurations are presented.

The linear induction accelerator is ideally suited for the production of an electron beam with several kA current and energy of a few MeV to several 10's of MeV. An induction accelerator is basically a one-to-one transformer in which the electron beam acts as the secondary. Its invention was stimulated by the desire to accelerate very high currents at high efficiency, which requires a low impedance device. To accomplish this the impedance of the transmission line cables is fed directly to the beam using a magnetic material as the isolation cores. The cores can then be stacked as shown in Fig. 1. This figure also indicates schematically the components of an FEL amplifier driven by an induction linac. The only challenge in producing electron beams suitable for driving an FEL amplifier is the condition of high-brightness. High current and high average power have been accomplished, as discussed in Sec. 2. In this paper we define the brightness in terms of the volume, δV^4, in 4D transverse phase space occupied by the beam to be

$$\mathcal{J}[\text{amp}/(\text{cm} - \text{rad})^2] = \frac{\pi^2 I}{\gamma^2 \delta V^4} \quad . \tag{1.2}$$

If the volume is a 4D elipsoid, $\delta V^4 = \pi^2 \epsilon_x \epsilon_y / 2$, with ϵ_x and ϵ_y the emittance in the two transverse planes. This definition is not universally employed.

II. THE INDUCTION ACCELERATOR

History

The first linear induction accelerator was constructed at Lawrence Livermore National Laboratory (then known as Lawrence Radiation Laboratory, Livermore) in the early 1960's. This machine was replaced by a new Astron accelerator in 1969 (Beal, et al., 1969). The purpose of these machines was to supply electrons for plasma confinement through magnetic field reversal from a cylindrical layer of circulating electrons. The second Astron accelerator and all other linear induction accelerators ever built in the USA are

listed in Table 1, along with the output beam parameters. The Astron accelerator has long since been retired, as has the ERA injector (Avery, et al., 1971). In fact, the ETA (Experimental Test Accelerator, Hester, et al., 1979) was constructed in the building previously containing the Astron accelerator. In retrospect, the Astron accelerator would have been a fine machine for FEL experiments with radiation wavelength of a few mm. At 500A, 5 MeV, the energy variation at the head and tail of the 300 ns pulse was 1/2%. During the pulse the energy spread and variation with time were not measurable. The emittance at 5 MeV was about 10 mrad-cm, so the brightness was of the order of 10^5 $A/(rad\text{-}cm)^2$. Even with antiquated technology, the repetition rate was impressive for short periods of time.

The National Bureau of Standards prototype consisted of one soft iron induction core providing a pulse length of 2 μs-(Leiss, et al., 1980). This device has since been moved to the Naval Research Laboratory where it is employed for various research projects, including FEL experiments. The FXR machine was built for flash x-ray radiography and is presently operated at Livermore (Kulke and Kihara, 1983).

The ETA operating at an energy of about 3.5 MeV and with output current reduced to ~ 3 kA is presently being used as the driver for the ELF experiment described in Sec. 4. The machine is to be replaced by an accelerator employing more modern technology, in particular a higher continuous pulse rate, reduced current, and higher brightness.

The ATA (Advanced Test Accelerator, Reginato, 1983) is presently being prepared to drive an FEL amplifier experiment called PALADIN. This experiment will use a wiggler with λ_w = 8 cm and a radiation wavelength of 10.6μ. It should be noted that high brightness was not a design goal in either ETA or ATA. The principal design goal was high current; an order-of-magnitude higher than previously achieved in induction linacs. The High Brightness Test Stand (HBTS, Caporaso and Birx, 1985) is an experimental test bed for pulsed power technology as well as cathode-anode geometry necessary to maximize beam brightness. In order to enhance the brightness in ATA, the cathode-anode geometry has been painstakingly redesigned (Boyd, et al., 1985). Only a small portion of the electron gun hardware need be replaced in order to implement this design.

Beam Breakup

The high current in these machines push against a very fundamental limit in all linacs, namely the beam breakup instability. The phenomenon exhibits unstable coherent transverse motion of the beam resulting from the excitation of transverse modes in the accelerating cells (R. K. Cooper, this conference). The induction machine has considerable advantage over rf linacs with regard to suppressing this instability because the cells are inherently very low Q structures. There is no necessity for highly resonant structures as in an rf linacs; the cells merely couple the drive cables to the beam. The induction core is ferrite, a very good microwave absorber. The cells are carefully shaped to suppress resonances, and additional ferrite inserted in strategic locations. But even if all resonances are destroyed, the very presence of the accelerating gaps lead to a resistive, or radiative, instability.

This problem limited the current in Astron to less than 1 kA, and was a well-recognized obstacle when ATA was constructed. It turned out that the focusing provided by the solenoidal transport coils was not sufficient to suppress the instability at full current (Chong, et al., 1985) but could probably do so at 2 or 3 kA required for the PALADIN experiment. We were seeking innovative solutions, and developed a technique called laser guiding.

Laser Guiding

In this technique (Martin, et al, 1985), a small diameter KrF laser beam passes through the center of the cathode and down the entire length of the machine. A background of benzene gas is fed into the machine from about the 5 MeV point at a pressure of approximately 10^{-4} torr. A small percentage of the gas is ionized by the KrF laser, the background electrons are expelled by the beam, and the remaining low density column of ions provides focusing forces that are far stronger than those provided by the solenoids. In addition, the focusing forces are nonlinear and introduce Landau damping, or phase mixing, which is sufficient to completely suppress the instability. The instability cannot be completely suppressed without phase mixing; it can only be made tolerable.

But laser guiding presents some undesirable side effects. The very phase mixing causes an inevitable emittance growth. The laser ionizes only a small fraction of the benzene molecules, and the beam electrons can ionize more. So

the focusing forces are time-dependent during the beam pulse, and a time-dependent emittance can result. But with a lower benzene pressure, a more powerful laser could ionize a much larger fraction of the molecules and leave few if any to be ionized by the beam electrons. Techniques for matching the beam onto and off of the ion channel have not been fully perfected. So although laser guiding reduced the instability in ATA to the extent that transverse oscillations cannot be detected, and the technique is undoubtedly a real breakthrough, it is not clear how useful it is when extremely high-brightness is essential.

III. ONE DIMENSIONAL FEL THEORY

A comprehensive 1D theory of the tapered-wiggler FEL amplifier was presented by Kroll, Morton and Rosenbluth (1981). The notation used here follows Prosnitz, et al., (1981). Here we will briefly review the theory with emphasis on the importance of small energy spread and high brightness. We employ Gaussian units in this section.

Particle Motion

The electric and magnetic fields we consider are the wiggler magnetic field B and the radiation electric field E of the form

$$\bar{B} = - B_w \sin k_w z \cosh k_w y \, \hat{y} \tag{3.1}$$

$$\bar{E} = E \sin (kz - \omega t + \phi) \, \hat{x} \quad , \tag{3.2}$$

in which $k_w = 2\pi/\lambda_w$, $k = 2\pi/\lambda$, $\omega = kc$ and ϕ is the phase of the radiation field. There are, of course, other field components, but these expressions will suffice for this simple treatment. We also set $\cosh k_w y = 1$.
For electrons the equation of motion is (with m the rest mass)

$$\frac{dv_x}{dz} = \frac{eB_y}{\gamma mc} \quad , \tag{3.3}$$

and therefore

$$v_x = \frac{eB_w}{\gamma mck_w} \cos k_w z \quad . \tag{3.4}$$

The change in energy of the electrons is determined by the equation

$$\frac{d\gamma}{dz} = -\frac{ev_x E_x}{mc^2 v_z}$$

$$= -\left(\frac{e}{mc^2}\right)^2 \frac{E_s B_w}{2\gamma k_w} \left\{\sin\left[(k + k_w)z - \omega t + \phi\right] + \sin\left[(k - k_w)z - \omega t + \phi\right]\right\} \quad . \tag{3.5}$$

We have set $v_z = c$ in this expression. The second term in { } in Eq. (3.4) represents a fast wave that can contribute little to the average energy change and therefore will be neglected.

We define the relative phase ψ to be

$$\psi = (k + k_w)z - \omega t + \phi \quad , \tag{3.6}$$

so that

$$\frac{d\psi}{dz} = k\left(1 - \frac{c}{v_z}\right) + k_w + \frac{d\phi}{dz} \quad , \tag{3.7}$$

and now v_z must be accurately determined. The radiation phase ϕ does change slowly with z as we shall see below, but we ignore $d\phi/dz$ in Eq. (3.6) to obtain the resonance condition

$$k[1 - (c/v_z)] + k_w = 0 \quad . \tag{3.8}$$

Physically, Eq. (3.7) states that as a particle travels one wiggler wavelength in z, the radiation travels a distance $\lambda_w + \lambda_s$. In terms of $\beta_z \equiv v_z/c$, the equation may be rewritten in the form

$$k_w = \frac{k(1 - \beta_z^2)}{\beta_z(1 + \beta_z)}$$

$$\approx \frac{k}{2}(1 - \beta_z^2) \quad . \tag{3.9}$$

A particle with v_z satisfying Eq. (3.9) maintains constant phase relative to the radiation wave, continually gaining or losing energy according to Eq. (3.5). We further have $1 - \beta_z^2 = 1 - \beta^2 + (v_x/c)^2$, where $\beta = v/c$ and v the total electron speed. Inserting Eq. (3.4) and averaging over one wiggler period, we have

$$1 - \beta_z^2 = \frac{(1 + a_w^2)}{\gamma^2} \quad , \tag{3.10}$$

in which we revert to conventional notation by introducing the quantity a_w by the definition

$$a_w = eB_w/\sqrt{2}mc^2 \, k_w \quad . \tag{3.11}$$

Equations (3.9) and (3.10) provide the resonance condition given in the introduction.

Energy Spread

We may write Eq. (3.7) in the form

$$\frac{d\psi}{dz} = k_w - \frac{k}{2\gamma^2}(1 + a_w^2) \quad . \tag{3.12}$$

Introducing the quantity e_s by the definition

$$e_s = eE_s/\sqrt{2}mc^2 \quad , \tag{3.13}$$

we may write Eq. (3.5) as

$$\frac{d\gamma}{dz} = -\frac{e_s a_w}{\gamma} \sin\psi \quad . \tag{3.14}$$

We define a resonant particle and attach a subscript r to quantities pertaining to this particle. We set $\psi_r = 0$ and $d\psi_r/dz = 0$, so that $2k_w\gamma_r^2 = k(1 + a_w^2)$. For particles with $\gamma \neq \gamma_r$, we set $\gamma = \gamma_r + \delta$ and linearize Eq. (3.12) to obtain

$$\frac{d\psi}{dz} = 2k_w \frac{\delta}{\gamma_r} \quad . \tag{3.15}$$

Taking the derivative of this equation and employing Eq. (3.14) with $\gamma = \gamma_r$ we obtain the so-called pendulum equation, namely

$$\frac{d^2\psi}{dz^2} + K^2 \sin\psi = 0 \quad , \tag{3.16}$$

in which

$$K^2 = 2e_s a_w k_w / \gamma_r^2 \quad . \tag{3.17}$$

Equations (3.14), (3.15) and (3.16) describe the motion in $\gamma - \psi$ phase space of particles in an untapered wiggler. The description is completely analogous to rf accelerator theory. Particles lying within a closed curve $P(\psi,\delta)$, called the separatrix, execute periodic oscillations (called synchrotron oscillations) about the synchronous particle. They undergo no average energy change. For an untapered wiggler as treated here, the separatrix is given by

$$P(\psi,\delta) = \pm \left(\frac{e_s a_w}{k_w}\right)^{1/2} (1 + \cos\psi)^{1/2} \quad . \tag{3.18}$$

Particles within the separatrix are said to be trapped. The separatrix is completely analogous to a stationary "bucket" in rf accelerator theory. From Eq. (3.18) we see that the maximum energy spread for trapped particles is $\Delta\delta = 4(e_s a_w/k_w)^{1/2}$, which varies as the square root of the radiation field amplitude E_s. The input radiation power density ($\propto E_s^2$) necessary to trap particles in the bucket varies as the 4th power of the energy spread, thus small energy spread is definitely desirable.

If particles are uniformly distributed in the bucket, no net kinetic energy is converted to radiation. But if particles initially are all in the upper half of the bucket, they will oscillate around to the bottom, losing energy which is converted to radiation. Saturation in an untapered wiggler occurs when oscillation continues until some particles are gaining energy ($\psi < 0$) while others are still losing energy ($\psi > 0$) so that the net energy conversion rate goes to zero. The saturation phenomena is considerably more complex if, as in the ELF experiment, the conversion is large and E_s increases rapidly. The bucket grows and more particles are trapped.

Without going through the mathematical details we simply state that in a tapered wiggler, we can still define a resonant particle with $\psi_r \neq 0$ and $d\psi_r/dz < 0$. The separatrix takes the familiar fish shape of a decelerating bucket in an rf accelerator. Particles still execute oscillations about the synchronous particle, but the entire bucket is moving down in energy, so that there is average energy conversion regardless of the distribution of trapped particles.

The Radiation Field

The energy converted to radiation can be calculated from the wave equation for E_y, namely

$$\frac{\partial^2 E_y}{\partial z^2} - \frac{1}{c^2}\frac{\partial^2 E_y}{dt^2} = \frac{4\pi}{c^2}\frac{\partial J_y}{\partial t} \quad . \tag{3.19}$$

This equation is solved in the slowly varying envelope approximation. That is, we assume that the amplitude E_s and the phase ϕ vary slowly with z. For E_y given by Eq. (3.2) and $\psi_s = kz - \omega t + \phi$, Eq. (3.19) becomes

$$2k\left[\frac{dE_s}{dz}\cos\psi_s - E_s\frac{d\phi}{dz}\sin\psi_s\right] = \frac{4\pi}{c^2}\frac{\partial J_y}{\partial t} \quad . \tag{3.20}$$

We note that in these units the impedance of free space is $4\pi/c$. To convert to practical units, replace this factor by $Z_o = 120\pi\Omega$. We do that in the following.

Only the Fourier components of J_y varying as $\sin\psi_s$ and $\cos\psi_s$ contribute to Eq. (3.20). In simulation codes such as FRED (which is briefly described in the following) these components are found by Fourier decomposing a particle distribution. In any case, the solutions to Eq. (3.20) are

$$\frac{dE_s}{dz} = \frac{Z_o}{\sqrt{2}}a_w J\left\langle\frac{\sin\psi}{\gamma}\right\rangle \quad , \tag{3.21}$$

$$\frac{d\phi}{dz} = \frac{Z_o}{\sqrt{2}}a_w\frac{J}{E_s}\left\langle\frac{\cos\psi}{\gamma}\right\rangle \quad . \tag{3.22}$$

In these expressions J is the total beam current density and $\langle\ \rangle$ indicates an average over all particles in the interval $-\pi < \psi < \pi$. Equations (3.21) and (3.22) describe the change in amplitude and phase of the radiation electric field. The change in amplitude has been demonstrated experimentally. The change in phase is such as to produce a focusing of the radiation. There has been experimental verification of the phase change in the ELF experiment, but the focusing can be definitively observed only in an experiment that is longer than the Rayleigh range.

Focusing in the x direction can be accomplished with quadrupole magnets, as is done in the ELF wiggler. Over the entire 3m length of the wiggler there is an air-core quadrupole focusing in the x direction. The defocusing in the y direction is small compared to the very strong edge focusing in that device. But the resulting betatron oscillations in the x direction are sinusoidal, and $\gamma\beta_{ex}$ is not constant over a betatron period, which causes little problem in ELF, but is generally undesirable.

There is a method for providing focusing in both x and y such that $a_w^2 + (\gamma\beta_e)^2$ remains constant over a betatron period. Again the method was recognized by Phillips, but invented independently by Scharlemann (1985). The details are a bit complicated, but the feat is accomplished by parabolic shaping of the wiggler pole faces to introduce a sextupole component into the wiggler magnetic field. This pole-face shaping is implemented in the PALADIN wiggler. Even though a particle will not move into and out of the bucket during a betatron period, finite emittance smears out the resonance, increases the input power required to trap particles, and decreases the efficiency of energy conversion.

IV. THE ELF EXPERIMENT

The parameters of the ELF experiment are given in Table 2. These parameters were chosen in part because ETA was available as a driver. Originally plans were to do experiments at λ_s = 4 mm and 2 mm as well as 8.6 mm. The application of the device to heat plasma in a magnetic confinement fusion experiment gave the device practical justification.

Theoretical support for FEL experiments is primarily provided by the computer code FRED (Fawley, et al., 1984 and Scharlemann, 1985). This code follows particles in one slice of the beam $-\pi < \psi < \pi$, or length ~ λ_s, through the wiggler. Particle trajectories are calculated in 3 dimensions, and the radiation field equations are solved in two dimensions, r and z in cylindrical coordinates for free space propagation, or x and z for propagation in a waveguide. In addition to the radiation fields, electrostatic forces from the spatially modulated charge density are included. These electrostatic forces are significant with the high current and low electron energy in the ELF experiment, but not in the forthcoming PALADIN experiment using ATA. In the following theoretical predictions are compared to experimental results, and generally found to agree very well.

Emittance

In all the above discussions, the transverse motion of particles arises only from the wiggler magnetic field. In practice particles have additional transverse velocity components from finite temperature, or emittance. A spread in transverse velocity has the same effect as a spread in energy in that both produce a spread in axial speed v_z, making it more difficult for particles to remain in phase with the radiation. The ramifications of finite emittance can be illustrated from equation $1 - \beta_z^2 = 1 - \beta^2 + (v_t/c)^2$. In the above v_t was merely v_x from the motion in the wiggler, and led to Eq. (3.12). But with finite emittance we have $\bar{v}_t = v_x \hat{x} + \bar{v}_e$, with $\bar{v}_e$ the random transverse velocity. If the betatron wavelength is much longer than λ_w, $\bar{v}_e$ does not change much over one wiggler period, the average of $v_x v_{ex}$ over a period is negligible, and Eq. (3.12) becomes

$$\frac{d\psi}{dz} = k_w - \frac{k}{2\gamma^2}\left[1 + a_w^2 + (\gamma\beta_e)^2\right] . \tag{3.23}$$

There are now some obvious complications. The resonance condition is different for particles with different β_e. Furthermore, depending on the focusing of transverse motion, β_e may change during a betatron oscillation. The particle may be inside the bucket during part of a betatron period and outside during the remainder. This observation brings us to the question of focusing within the wiggler.

Along with the wiggler magnetic field given by Eq. (3.1) there is a B_z given by

$$B_z = - B_w \cos k_w z \sinh k_w y . \tag{3.24}$$

The force in the y direction resulting from $v_x B_z$, with v_x given by Eq. (3.4), gives a net focusing force in the y direction. This focusing, known as edge focusing in beam transport theory, was recognized by Phillips (1960). There is no focusing in the x direction. However, a_w varies with y through the factor $\cosh k_w y$. For betatron motion in the y direction only, the variation of a_w and β_e are such that $a_w^2 + \gamma^2\beta_e^2$ is constant over a betatron oscillation. A particle with velocity $v_{ye} \neq 0$, $v_{xe} = 0$ may have a different resonance condition than one with $v_{ye} = v_{xe} = 0$, but at least the condition remains constant over a betatron period.

Hardware

The experimental setup is described by Orzechowski, et al. (1983). A schematic drawing of the wiggler magnet surrounded by the air-core quadrupoles is shown in Fig. 2. Experiments use a 3 kA current out of ETA at about 3.5 MeV. An emittance filter in the beamline selects a known value of δV^4 and transmits up to 1.2 kA with a brightness of 2 x 10^4A/(cm-rad)^2. The electron beam pulse through the wiggler is 12 to 15 ns duration. The wiggler wavelength is uniform in z, but each two periods of the wiggler are individually controlled, allowing tapering and variation of the interaction length in the untapered experiments. The input signal is generated by a 35 GHz magnetron, delivering up to 50 kW for a period of 500 ns.

Untapered Wiggler

Experimental techniques and results of the experiments with the untapered wiggler are given by Orzechowski, et al. (1986). The small signal gain (growth from noise) is shown in Fig. 3, which indicates a gain of 26.6dB/m. The extrapolated input noise level is 1.5 mW.

Amplifier performance was studied as a function of wiggler length. The length is varied by tuning the downstream portion of the wiggler field so that it is significantly off resonance and does not contribute to the FEL interaction. (A low magnetic field is necessary to focus the beam.) Experimental results are indicated by the circles in Fig. 4. The initial exponential growth is about 34dB/m, somewhat higher than the small signal gain. Saturation occurs at about 1.4 m at an output power level of 150 MW. Up to 180 MW has been achieved. The saturated output power shows very little dependence on input power from 3 to 30 kW. By varying the electron beam current, the saturated power is found to vary as I^2, and this is one of the aspects of saturation that is not fully understood.

Comparison of experimental results with code calculations for the untapered wiggler has been presented by Scharlemann, et al, (1986). Results of simulation of the amplifier are shown as the solid curve in Fig. 4. There is one caveat in that the experiment used B_w = 3.8 kG while the code results were obtained for 3.65 kG. There is a discrepancy in the post-saturation power oscillations. These oscillations are probably a manifestation of coherent synchrotron oscillations, and the discrepancy probably arises from inadequate treatment of the electrostatic field by the simulations.

Tapered Wiggler

Saturation occurs in the untapered wiggler because particles lose energy and fall out of resonance. By tapering (reducing) the wiggler magnetic field the resonance condition can be maintained. Experimentally the optimum taper was found by maintaining the untapered configuration to the saturation point (taking advantage of the exponential gain) and then turning up B in each subsequent two-period segment of the wiggler to maximize the output power. This procedure determines the taper while increasing the wiggler length. The tapered wiggler experiment is described by Orzechowski, et al., (1986) and the results are shown by the + in Fig. 5. The peak electron beam current was 1.1 kA in this experiment. Experimentally the peak output power reached 1.5 GW, an order of magnitude more than achieved in the untapered wiggler, and corresponding to a conversion (extraction) efficiency of 40%.

Using the experimentally determined taper, the simulation produced results shown by the upper solid curve in Fig. 5. The lower circles and solid curve in Fig. 5 are the same as shown in Fig. 4 for the untapered wiggler.

Table 1

Electron Induction Linacs in USA

	Kinetic energy	Beam current	Pulse length	Avg. rep. rate (max)	Burst rep. rate
Astron injector, LLNL Original (1963)	3.7 MeV	350 A	300 ns	60 Hz	360 Hz for 7 pulses
Upgrade (1968)	6 MeV	800 A	300 ns	60 Hz	800 Hz for 100 pulses
NBS prototype (1971)	0.8 MeV	1,000 A	2,000 ns	1 Hz	-
ERA injector LBL (1971)	4 MeV	1,000 A	45 ns	5 Hz	-
ETA, LLNL (1979	4.5 MeV	10,000 A	30 ns	2 Hz	900 Hz for 5 pulses
FXR, LLNL (1982)	18 MeV	3,000 A	70 ns	0.3 Hz	-
ATA, LLNL (1983)	45 MeV	10,000 A	60 ns	5 Hz	(1,000 Hz for 10 pulses)
HBTS, LLNL (1984)	1.5 MeV	2,000 A	60 ns	100 Hz (1,000 Hz)	

Table 2

ELF Operating Parameters

Wiggler	
Period (cm)	9.8
Length (m)	2.94
Number of periods	30
Peak magnetic field (kG)	0-5 (adjustable)
Horizontal focusing quadrupole strength (G cm^{-1})	30-60
Electron beam	
Kinetic energy (MeV)	3.0 - 3.5
Current (A)	850
Unnormalized edge emittance (mrad-cm) ($\varepsilon \equiv x_{max}x'_{max}$)	70
Equilibrium beam cross-section (cm) (in wiggler)	0.6 x 1.2
Current density profile	$\propto \left[1 - \frac{x^2}{x_{max}^2} - \frac{y^2}{y_{max}^2}\right]$
Microwaves	
Frequency (GHz)	34.6
Waveguide size (cm)	3 x 10 cm
Input power (kW)	50
Design mode	TE_{01}

References

1. Avery, R., Behrsing, G., Chupp, W., Faltens, A., Hartwig, E.C., Hernandez, H.P., Macdonald, C., Meneghetti, J.R., Nemetz, R.G., Popenuck, W., Salsig, W. and Vanecek, D., Proc. of the 1971 Part. Acc. Conf. IEEE Proc. Nuc. Sci. NS-18 #3, 479 (1971).
2. Beal, J.W., Christofilos, N.C. and Hester, R.E., Proc. of the 1969 Part. Acc. Conf. IEEE Trans. Nuc. Sci. NS-16 #3, 294 (1969).
3. Boyd, J.K., Caporaso, G.J. and Cole, A.G., Proc. of the 1985 Part. Acc. Conf. IEEE Trans. Nuc. Sci. NS-12 #5, 2602 (1985).
4. Caporaso, G.J. and Birx, D.L., Proc. of the 1985 Part. Acc. Conf. IEEE Trans. Nuc. Sci. NS-32 #5, 2608 (1985).
5. Chong, Y.P., Caporaso, G.J. and Struve, K.W., Proc. of the 1985 Part. Acc. Conf. IEEE Trans. Nuc. Sci. NS-12 #5, 3210 (1985).
6. Fawley, W.M., Prosnitz, D. and Scharlemann, E.T., Phys. Rev. A30, 2472 (1984).
7. Hester, R.E., Bubp, D.G., Clark, C., Chesterman, A.W., Dexter, W.L., Fessenden, T.J., Reginato, L.L., Yakota, T.T. and Faltens, A.A., Proc. of the 1979 Part. Acc. Conf. IEEE Trans. Nuc. Sci. NS-26 #3, 4180 (1979).
8. Kroll, N.M., Morton, P.L. and Rosenbluth, M.N., IEEE Journal Quantum Electronics 17, 1436 (1981).
9. Kulke, B. and Kihara, R., Proc. of the 1983 Part. Acc. Conf. IEEE Trans. Nuc. Sci. NS-30 #4, 3030 (1983).
10. Leiss, J.E., Norris, N.J. and Wilson, M.A., Part. Acc. 10 223 (1980).
11. Martin, W.E., Caporaso, G.J., Fawley, W.M., Prosnitz, D., and Cole, A.G., Phys. Rev. Letters 54, 685 (1985).
12. Orzechowski, T.J., Prosnitz, D., Halbach, K., Kuenning, R.W., Paul, A.C., Hopkins, D.B., Sessler, A.M., Stover, G., Tanabe, J., and Wurtele, J.S., "A High Gain Free Electron Laser at ETA" Lawrence Livermore National Laboratory Report UCRL-88705 (1983).
13. Orzechowski, T.J., Anderson, B.R., Fawley, W.M., Prosnitz, D., Scharlemann, E.T., Yarema, S.M., Sessler, A.M., Hopkins, D.B., Paul, A.C., and Wurtele, J.S., Proceedings of the Seventh International Free Electron Laser Conference, E.T. Scharlemann and D. Prosnitz, eds., Nuclear Instruments & Methods A249 (1986), in press.

14. Orzechowski, T.J., Anderson, B.R., Clark, J.C., Fawley, W.M., Paul, A.C., Prosnitz, D., Scharlemann, E.T., Yarema, S.M., Hopkins, D.B., Sessler, A.M., and Wurtele, J.S., Lawrence Livermore National Laboratory Report UCRL-53738 (1986). Submitted for publication in Phys. Rev. Letters.
15. Phillips, R.M., IRE Trans. on Electron Devices 7, 231 (1960).
16. Prosnitz, D., Szöke, A. and Neil, V.K., Phys. Rev. A24, 1436 (1981).
17. Reginato, L.L., for the ATA Staff, Proc. of the 1983 Part. Acc. Conf. IEEE Trans. Nuc. Sci. NS-30 #4, 2970 (1983).
18. Scharlemann, E.T., Jour. App. Phys. 58, 2154 (1985).
19. Scharlemann, E.T., Fawley, W.M., Anderson, B.R., and Orzechowski, T.J., Proc. of the Seventh International Free Electron Laser Conference, E.T. Scharlemann and D. Prosnitz, eds., Nuclear Instruments & Methods A249 (1986), in press.

Figure Captions

1. The components of an FEL amplifier driven by an induction linac.
2. Cross section of interaction region showing orientation of wiggler field and electron oscillation. The TE_{10} mode is excited in the waveguide. Quadrupole magnets stabilize the electron orbits in the horizontal plane.
3. Small signal gain in the super-radiant mode as a function of wiggler length. Extrapolating the signal back to the origin gives an effective input signal of 1.3m W.
4. TE_{01} power vs. wiggler length. The circles are experimental data; the solid line is the result of simulation.
5. Results of experiment and simulation for the tapered and untapered wiggler, the latter taken from Fig. 4.

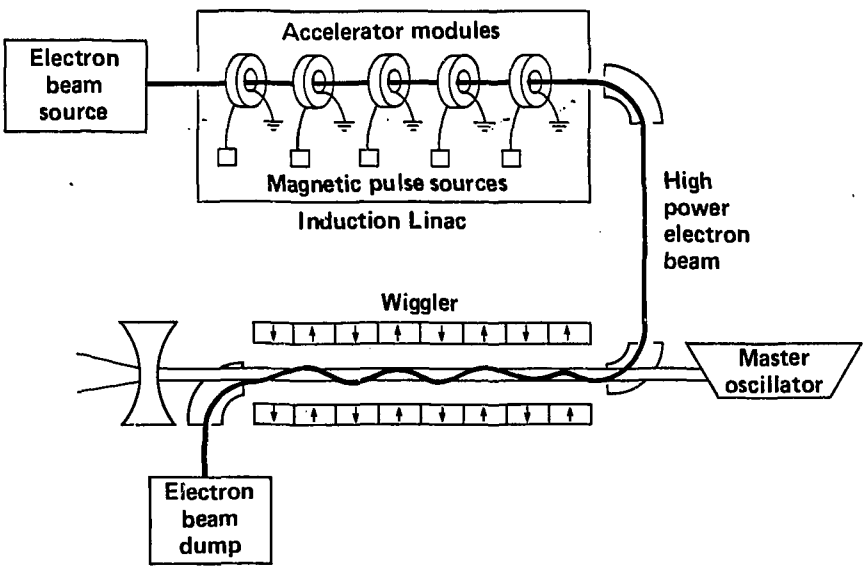
Accelerator modules
Electron beam source
Magnetic pulse sources
Induction Linac
High power electron beam
Wiggler
Master oscillator
Electron beam dump

Figure 1

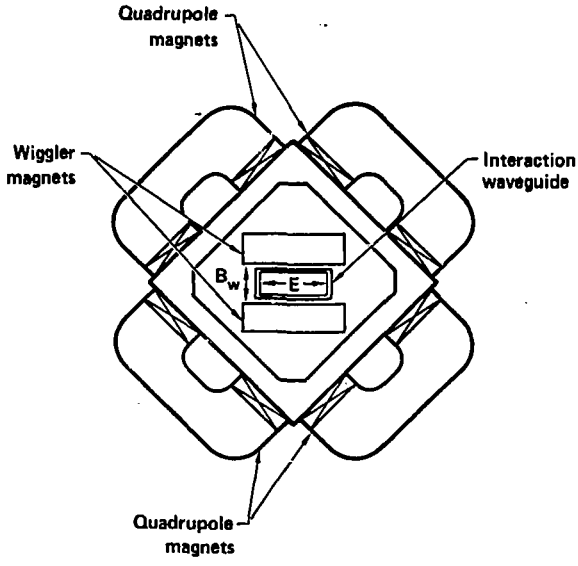
Quadrupole magnets
Wiggler magnets
Interaction waveguide
B_w
E
Quadrupole magnets

Figure 2

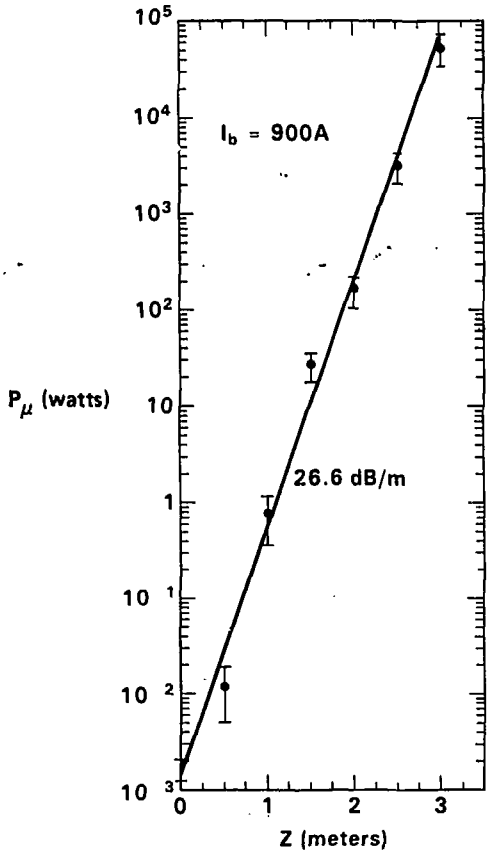
10^5
10^4
10^3
10^2
10
1
10^{-1}
10^{-2}
10^{-3}
I_b = 900A
26.6 dB/m
P_μ (watts)
0
1
2
3
Z (meters)

Figure 3

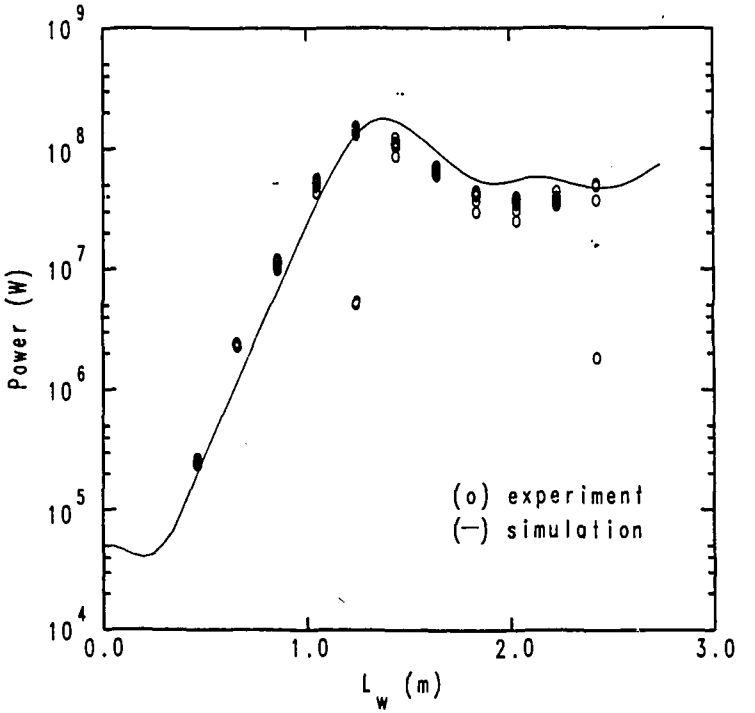
Power (W)
10^9
10^8
10^7
10^6
10^5
10^4
0.0
1.0
2.0
3.0
L_w (m)
(o) experiment
(—) simulation

Figure 4

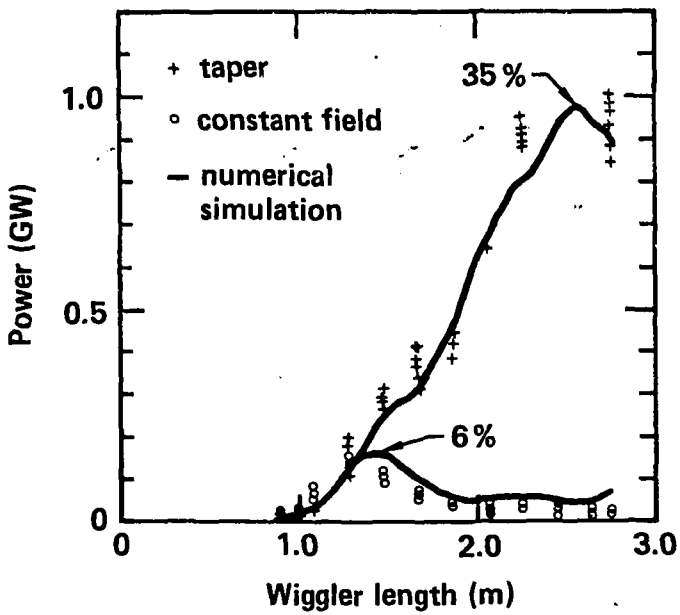
+ taper
° constant field
— numerical simulation
35 %
6 %
1.0
0.5
0
Power (GW)
0
1.0
2.0
3.0
Wiggler length (m)

Figure 5